ANALYSIS OF HEAT FLOW ALONG A TRANSECT ACROSS THE SOUTH CHINA SEA

He Lijuan
Institute of Geology, Chinese Academy of Sciences
Beijing 100029
P.R. CHINA

ABSTRACT

The western transect across the South China Sea passes from the northern margin, across the slope, and into the central deep-sea basin, extending about 900 km. Substantial but highly scattered heat flow data have been collected along this transect. Systematic analysis of these data can identify the underlying geothermal conditions and their formation mechanism. First, trend analysis is used to determine the regional heat flow. The results show a high background heat flow with an average value of about 65-70 mW/m^2 in the northern part and 80 mW/m^2 in the central part of the transect. The heat flow increases from the northern margin to the deep-sea region, reaches its highest value in the Central Basin, and then decreases gradually, exhibiting a typical characteristic of rifting area. Secondly, a hydrothermal circulation mechanism may explain local anomalies in the heat flow data. A numerical model study suggests that hydrothermal convection within a highly permeable horizontal layer which is linked to the surface through open faults can explain the heat flow scatter.

1. INTRODUCTION

The South China Sea is a Cenozoic basin formed by multiple episode rifting and sea-floor spreading. The multi-phase extensional tectonic events and the generation of new oceanic crust have resulted in a high heat flow and elevated crustal temperatures, as has been shown by studies of the regional heat flow (He et al., 1998) and tectono-thermal modeling of the temperature field (Nissen et al., 1995a; He et al., 1995). An unusual feature of the heat flow in the South China Sea is a large scatter in the observed values which cannot be attributed to measurement errors or annual variation in sea bottom temperatures (Nissen et al., 1995a). Such small-scale variability cannot be explained by conventional lithospheric-scale extensional models and suggests that the regional temperature field is strongly disturbed by some geological process that is not well understood. Hydrothermal circulation could possibly provide an explanation, because it can cause significant local deviations from the regional heat flow trend.

This paper aims to analyze the heat flow scatter along a geophysical transect across the northern margin of the South China Sea. Many geophysical and geological surveys have been carried out in the South China Sea, and three geophysical transects across the northern margin provide a particular good basis for

crustal studies (Yao et al., 1994). The westernmost transect, referred to as the western transect, is studied in this paper (Figure 1). It extends about 900 km from the northern margin, across the slope, and into the central deep-sea basin. An integrated geophysical survey, two-ship seismic, magnetic, gravity and heat flow data, were measured along this transect (Yao et al., 1994). Studies of the transect have led to a better understanding of the deep crustal structure and regional tectonic movements, but no study of the local hydrothermal circulation has been carried out. In this paper hydrothermal circulation within the sediment and/or basement is simulated using 2-D numerical model and the potential of this mechanism to generate the observed heat flow distribution is investigated.

2. GEOLOGICAL SETTING

The South China Sea lies to the south of the China mainland, and to the north of Borneo (Figure 1). It is bounded on the west by the Indochina Peninsula and the east by Luzon and the Philippines. During the Cenozoic, this basin experienced several episodes of extension and sea-floor spreading, directed NW-SE
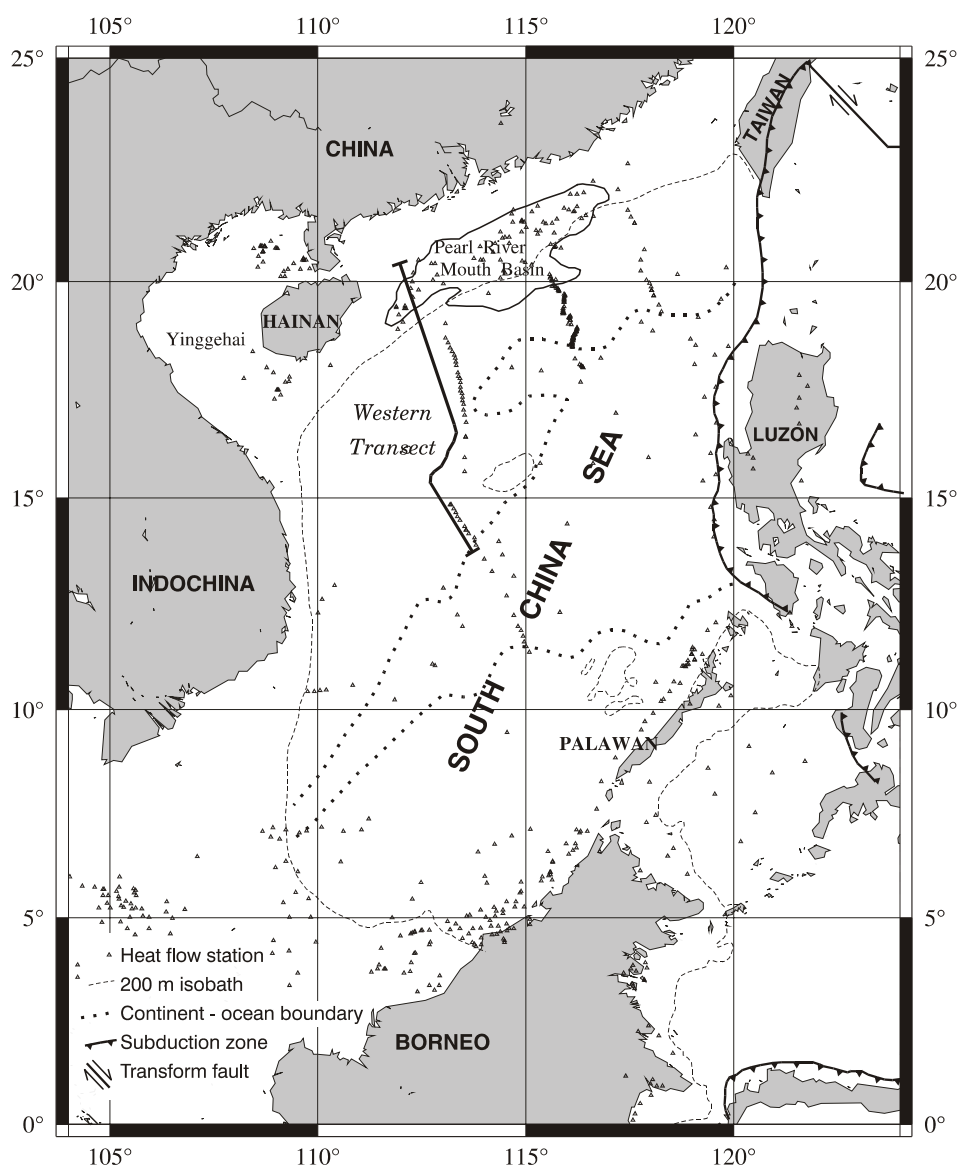

FIGURE 1: Map of the South China Sea,
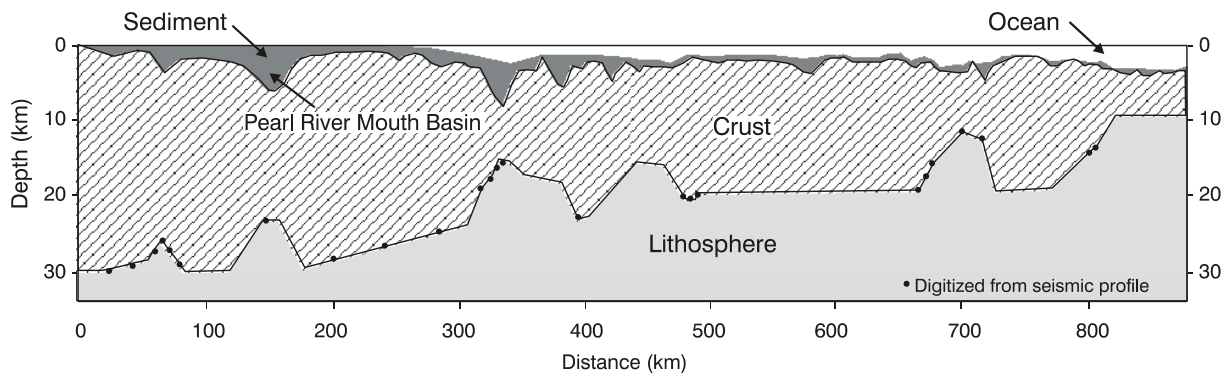also shown is the location of the western transect

FIGURE 2:   Crustal profile along the western transect based on a combination of two-ship seismic
refraction experiments and gravity modelling (modified from Nissen et al., 1995a)

to N-S. The timing of the extension episodes is, however, still somewhat uncertain. According to Yao et al. (1994), four phases of extension affected this region, beginning approximately at 54 Ma, 36 Ma, 15.2 Ma and 5.2 Ma (Ma = million years from present). During the last 1.9 Ma, thermal subsidence (contraction) has dominated in this area. Several stages of magmatism have been identified, the latest of which is of Post-Miocene age (Li and Rao, 1994).

As a result of strong extension and sea-floor spreading, the crust of South China Sea is very thin. Based on the results of two-ship seismic refraction experiments (ESP) in conjunction with gravity data, the large-scale crustal thickness variations have been deduced across the western transect (Figure 2). The crustal thickness (measured from the top of prerift basement to the Moho) ranges from 30 km to 8 km. It generally decreases southward across the south China margin but anomalously thin crust, overlain by thick sedimentary sections, has also been identified at two other locations (Nissen et al., 1995b).

Reflection seismic and well data show the stratigraphy in the Pearl River Mouth Basin, at the northern end of the western transect (Figure 1). Both Paleocene and Eocene strata comprise mainly organic-rich mudstones (Yu, 1994). The overlying early Oligocene sequence is composed of flood plain mudstones, coal seams and silty sandstones, whereas the late Oligocene deposits are dominated by kaolinitic sandstones, bituminous shale and coal. The Miocene strata are divided into three formations: Zhujiang conglomerates, sandstones, bituminous shale and coal limestones; Hanjiang sandy conglomerates, sandstones and mudstones; and Viethai fine sandstones, conglomerates, mudstones and clayey siltstones. From the Pliocene, sandy conglomerates, clayey siltstones and mudstones were deposited in the area.

3. GEOTHERMAL BACKGROUND

The overall geothermal regime of sedimentary basins is controlled by regional tectonic processes and heat flow measurements are a powerful tool for studying this regime. In the South China Sea, the geothermal regime was shaped by multi-phase extension and crustal thinning.

At present, 584 heat flow measurements are available from the South China Sea. The heat flow values range from 8 mW/m^2 to 191 mW/m^2, with an average value of 77.0 mW/m^2. If values below 30 mW/m^2 are excluded the average value becomes 78.3 mW/m^2 (He et al., 1998). This is much higher than the mean value (65.2 mW/m^2) for the continental area in China.

Figure 3 shows a heat flow contour map of the South China Sea, which was constructed by the GMT software (Wessel and Smith, 1995). The highest heat flow is found over young oceanic crust in the center of the basin. The two maxima are located over the relict spreading center. The heat flow increases gradually from the northern margin southward to the central basin, as is to be expected from the basinward thinning of the crust (Figure 2).
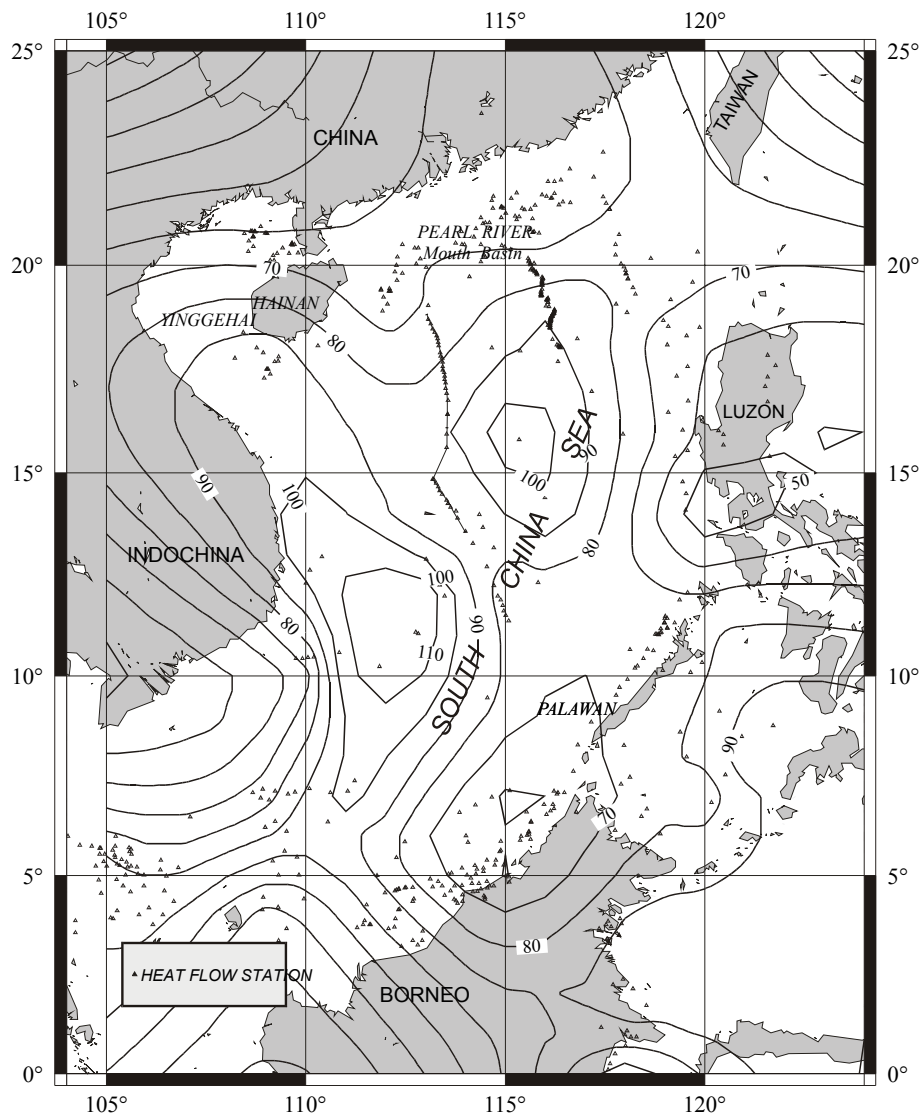
FIGURE 3:   Heat flow contour map of the South China Sea

4. HEAT FLOW

4.1 Heat flow data and trend analysis

For the present study, 63 heat flow measurements were available along the western transect, 23 from the Pearl River Mouth Basin, and 40 from the Conrad c2614 cruise (Nissen et. al., 1995a). Temperature gradients were measured over a subsurface depth range of ~5 m with up to six thermistors and were found to be linear to within the measurement error of the thermistors (±0.005°C). The thermal conductivity, which must be known in order to calculate the heat flow, was measured by a needle probe technique on five cores raised from roughly equally spaced intervals up the continental slope. The heat flow values collected along the transect are highly scattered (Figure 4). According to Nissen et. al. (1995a), this scatter can neither be attributed to measurement errors nor to temperature perturbations caused by annual variations in seafloor temperatures.

In order to determine the heat flow trend along the western transect, several 1-D polynomials were fitted to the data. A 3rd order polynomial fit is shown in Figure 4. The heat flow increases from the northern margin (0-200 km) to the deep-sea region, reaches its highest value in the central basin (400-500 km), and then decreases gradually. The average value is about 65-70 mW/m^2 at the northern margin, and 80 mW/m^2 in the central part of the transect. In general, the heat flow shows the typical characteristic of
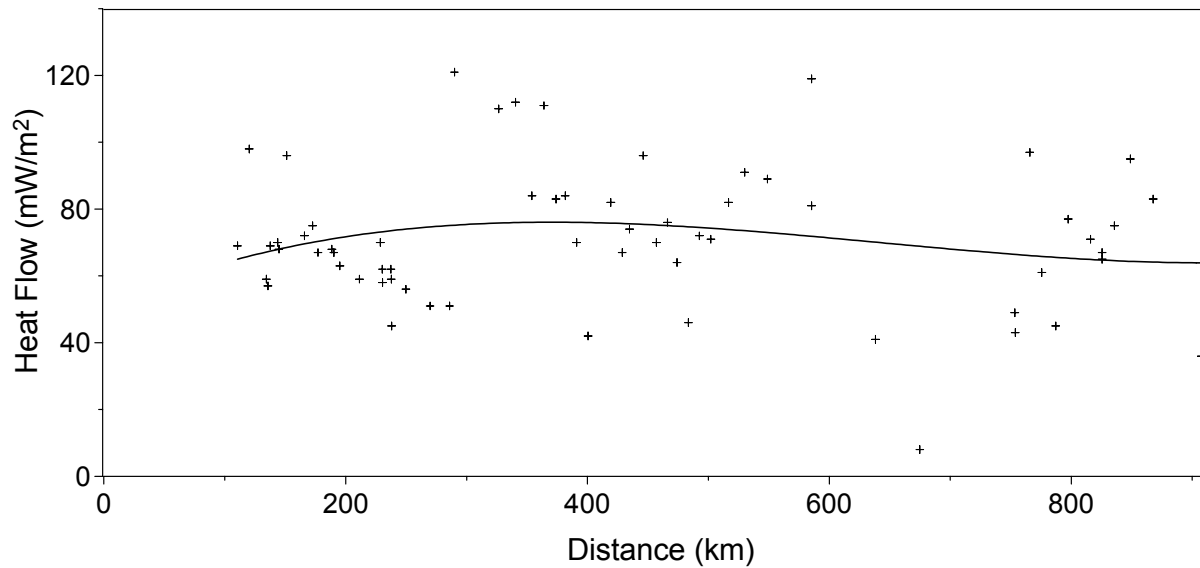
FIGURE 4:   Heat flow along the western transect

rifted areas; i.e. the heat flow is high near the rift axis, and then decreases with increasing distance away from it.

The heat flow trend represents the background heat flow caused by lithospheric extension and sea-floor spreading. There is scatter of values around the trend and it is tempting to regard it as noise. However, the scatter is so large that in order to understand the geothermics of the basin, explanation is required. Two mechanisms are commonly cited as plausible explanation for the scatter. One is hydrothermal circulation at shallow depth in the sediments and/or basement. The other is intrusion of magma into the crust. In the following, a numerical simulation technique is used to investigate whether the scatter of the data can be explained in a satisfactory way by hydrothermal circulation. The software used is TOUGH2, developed by Pruess (1991). The TOUGH2 code is a general-purpose and thoroughly tested numerical simulation program for multi-dimensional fluid and heat flow of multi-phase, multi-component fluid mixtures in porous and fractured media.

4.2   Estimation of crustal temperature distribution

Before simulating the local heat flow anomalies, a model of the regional temperature field was constructed. The model provides a realistic physical explanation for the regional heat flow trend and, thus, underpins the proposed separation of anomalous heat flow from the regional background.   More importantly, it provides boundary conditions for detailed submodels, which will be used to investigate local anomalies in the heat flow.

For the calculations, we selected a 400 km long and 10 km deep section, divided into crust and sediments as shown in the northern half of Figure 2. As the model is only two-dimensional and neglects fluid convection, the temperature field is governed by the 2-D heat conduction equation

$$\rho c \frac{\partial T}{\partial t} - \left(\frac{\partial^2 \lambda T}{\partial x^2} + \frac{\partial^2 \lambda T}{\partial y^2} \right) = Q \tag{1}$$

where T = Temperature;
   λ = Thermal conductivity;
   ρ = Density;
   c = Specific heat capacity;
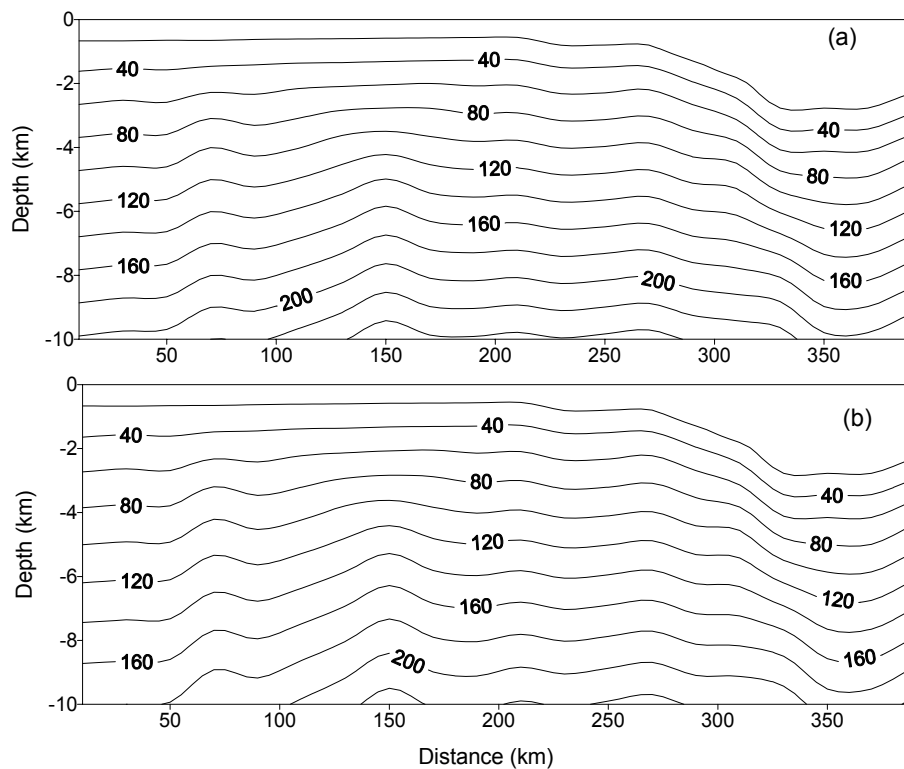 Q = Radiogenic heat production.

FIGURE 5:   Modeled regional temperature field along the northern part of
the western transect; a) Without radiogenic heat production from sediments
     and crust; b) With radiogenic heat production in sediments and crust

The upper model boundary was assumed to have a constant temperature of 4°C and no heat flow was allowed across the two vertical boundaries (i.e. $\partial T/\partial y = 0$). The lower boundary was assumed to have constant but unknown temperature. These have to be determined along the base of the 2D model.

The field data to be simulated is the regional heat flow profile in Figure 4. The TOUGH2 code was used to calculate the regional tempe-rature field distri-bution in the 2-D model assuming the thermal conductivity of the sediments and the crust to be 2.5 W/mK and 3.1 W/mK, respectively. It was further assumed that heat was transferred only by conduction. The regional temperature field obtained by ignoring radiogenic heat production in the sediments and crust is shown in Figure 5a. The simulated model base temperature increases southward, reaching its highest value at about 159 km from the origin of the profile, and then decreases gradually to the south, although the surface heat flow shows an increase all the way from north to south. This is because of the non-uniform geological structure of the model, which includes variations in topography and basement depth, and because of the contrast in thermal conductivity between the sediments and the crust.

If radiogenic heat production in the sediments and crust is added to the model ($1.5\,\mu\,W/m^3$), the calculated regional temperature field becomes as shown in Figure 5b. The temperature distribution is rather similar to Figure 5a. There is, however, a systematic difference in the temperature values. The introduction of radiogenic heat production lowers the temperature values in deeper parts of the model, because the surface heat flow is fixed. Since radiogenic heat production data are lacking, a reasonably constant value was adopted in order to show the influence of radiogenic heat production on the temperature field of the basin and crust. A comparison of Figures 5a and 5b shows that the temperature difference increases with depth. But at shallow depth in the sediments, the difference is very small. So it seemed reasonable to use a constant value for the radiogenic heat production as long as the root of the heat flow anomalies is shallow.

The calculated temperature field can be regarded as the background temperature field of the region. Generally, the regional temperature field is disturbed by local effects, which results in departures from the background. Hydrothermal convection has the potential to greatly disturb the regional temperature field as will be shown in next chapter.

5. EFFECTS OF HYDROTHERMAL CONVECTION ON SURFACE HEAT FLOW

In calculating the regional temperature field in Figure 5, only heat conduction was taken into account. Heat conduction and heat convection always coexist and transfer heat jointly at shallow depths in the crust, especially in sediments where permeability is relatively high. Water is a good carrier of heat, so heat transport by convection of liquid water through porous, permeable rocks is much faster than heat transport by conduction. The presence of local convection may cause large departures from the regional temperature field dominated by heat conduction, and this may lead to anomalous heat flow at the surface. At some geothermal sites, near-surface fluxes of 200-600 mW/m^2 can be found in up-flow zones whereas conduction-controlled background values are typically 60-80 mW/m^2 (Rybach and Muffler, 1981). However, in the recharge or down-flow zones, low or even zero thermal gradients can be observed. Hydrothermal convection is common in the oceanic crust, especially at and near the spreading ridge axis (Crane, 1979; Fehn and Cathles, 1979). For these reasons, it is highly relevant to investigate whether hydrothermal convection can explain the scatter of heat flow data along the western transect.

5.1 Balance law for liquid flow through porous media

The governing equations for single-phase fluid flow through porous media can be written in the form of balance laws.

Mass balance of fluid:

$$\nabla \cdot q = 0 \tag{2}$$

Momentum balance of fluid:

$$\nabla \cdot p - \rho_f g + \frac{\upsilon_o \sigma \rho_o}{\kappa} q = 0 \tag{3}$$

Energy balance of rock-fluid mixture:

$$[(1-\phi)\rho_r c_r + \phi \rho_o c_f]\frac{\partial T}{\partial t} + \rho_o q c_f \cdot \nabla T = \nabla \cdot (\lambda_m \nabla T) \tag{4}$$

where

a_f	= Coefficient of thermal expansion	
c_r	= Constant volume heat capacity of rock	
c_f	= Constant volume heat capacity of fluid	
g	= Acceleration due to gravity	
λ_m	= Mixture (rock and liquid) heat conductivity	
κ	= Permeability	
p	= Pressure	
q	= Volume flux vector for liquid	
t	= Time	
T	= Temperature	
ρ_i*	= Density	
ϕ	= Porosity	
υ	= Viscosity, $\upsilon = \upsilon_0 \sigma(T)$, $\sigma(T)$ is a prescribed function of temperature; and υ_o is the reference viscosity at reference temperature;	
$i*$	= f for fluid; r for rock; and o for initial or reference value	

The balance laws form a basis for numerous studies of fluid convection in porous media. Usually the convection of underground water can be divided into two kinds: free convection and forced convection (Wang Jiyang et al., 1993).

Free convection, also called thermal convection, is caused by temperature differences within a porous medium. Whether convection will occur depends on the Rayleigh number which, in the case of a horizontal porous layer, is defined as (Turcotte and Schubert, 1982)

$$Ra = \frac{\alpha_f g \rho_f^2 c_f \kappa b (T_l - T_u)}{\upsilon \lambda_m} \tag{5}$$

where b = Thickness of the porous layer;
T_u, T_l = Temperatures of the upper and lower boundaries, respectively.

Only when the Rayleigh number is greater than the critical Rayleigh number Ra_c can free convection occur. Ra_c depends on the material properties and boundary conditions of the model, but the most commonly cited value for a constant viscosity model heated uniformly from below is $4\pi^2$. Forced convection is driven by an external force. The velocity of the flow depends on the pressure gradients in the formation fluid, its viscosity and on the permeability of the solid medium.

5.2 Plausible models

Before modeling begins, a conceptual model is usually developed. This consists of a well-defined geometrical system with boundaries in which appropriate thermal and hydrological conditions can be applied, an internal structure consistent with local geology, and material properties of rock and water. A detailed conceptual model requires data from geophysical and geological surveys, and preferably, from drilling. In fact, it is often difficult to obtain all the data required, and the conceptual model has to be simplified. This problem was met in the South China Sea. Detailed data were lacking on geological features, such as the presence of faults in the sediments, and on the material properties of different formations. As a result, it was only possible to present simplified models of hydrothermal circulation. However, the models are plausible, and allow inferences to be made about the existence of convection and its influence on the surface heat flow.

5.2.1 Model A

According to borehole data from the Pearl River Mouth Basin, the sedimentary formations mainly consist of sandstone and mudstone. Sandstone is often a good aquifer and can retain high permeabilities to large depths. Measurements on core samples and sidewall cores show that there is a 700 m thick highly-permeable layer at depth of 3000-3700 m in the basin. Its average permeability is about 5.0×10^{-14} m^2 (Figure 6). These permeabilities form the basis of model-A (Figure 7) which has two types of media, a 700 m thick high-permeability layer with a
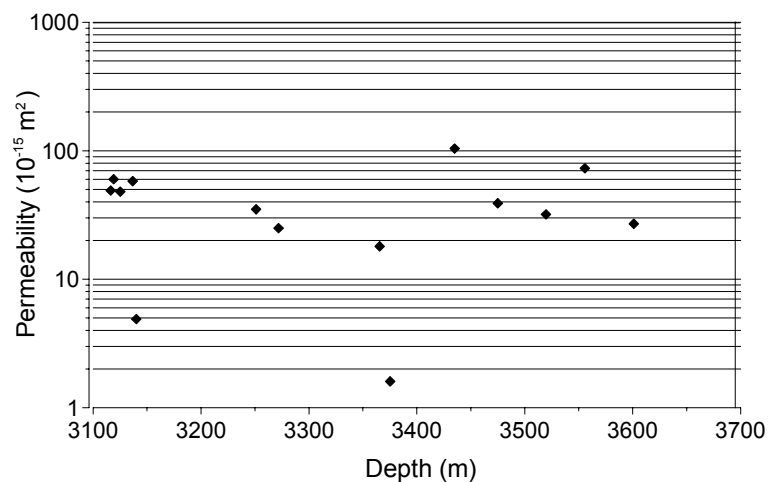
FIGURE 6: Permeabiblity measurements from well WC14-1-1 in the Pearl River Mouth Basin
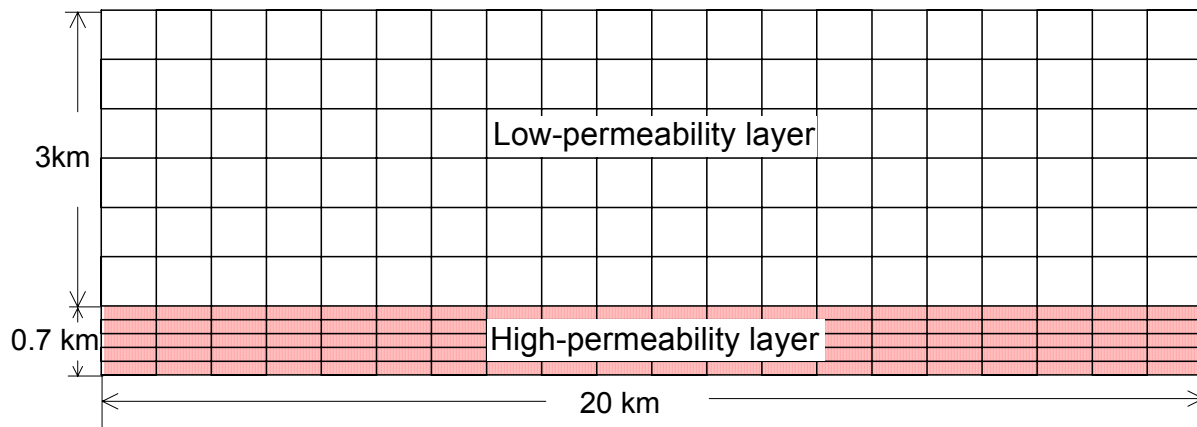
FIGURE 7:   Sketch of model A and grids used for modelling

permeability of 5.0×10^{-14} m^2 overlain by a 3000 m thick low-permeability layer with a permeability of 1.0×10^{-18} m^2. A constant temperature of 130°C was imposed at the lower boundary. This model yielded a surface heat flow of 68 mW/m^2 when only heat conduction was allowed, consistent with the regional heat flow of the basin. The temperature of the upper boundary was kept at 4°C. Parameter values used for the model are listed in Table 1.

TABLE 1:   Rock properties in models A and B

	Permeability (m^2)	Thermal conductivity (W/m·K)	Density (kg/m^3)	Heat capacity (J/kg·K)
Low-permeability layer	1.0×10^{-18}	2.0	2650	850
High-permeability layer	5.0×10^{-14}	2.0	2650	850
Fault	5.0×10^{-14}	2.0	2650	850

In this model, local convection will occur in the high-permeability layer. The occurrence of convection will distort the conductive temperature field. Figure 8 shows the stable temperature field in this case. The figure shows clearly that the temperature field in the high-permeability layer is disturbed and very different from the temperature field in the upper layer, which is dominated by heat conduction.

The convection also influences the heat flow, but the degree of influence changes significantly with depth. The average surface heat flow increases from 68.0 mW/m^2 to about 68.3 mW/m^2, and shows little variations
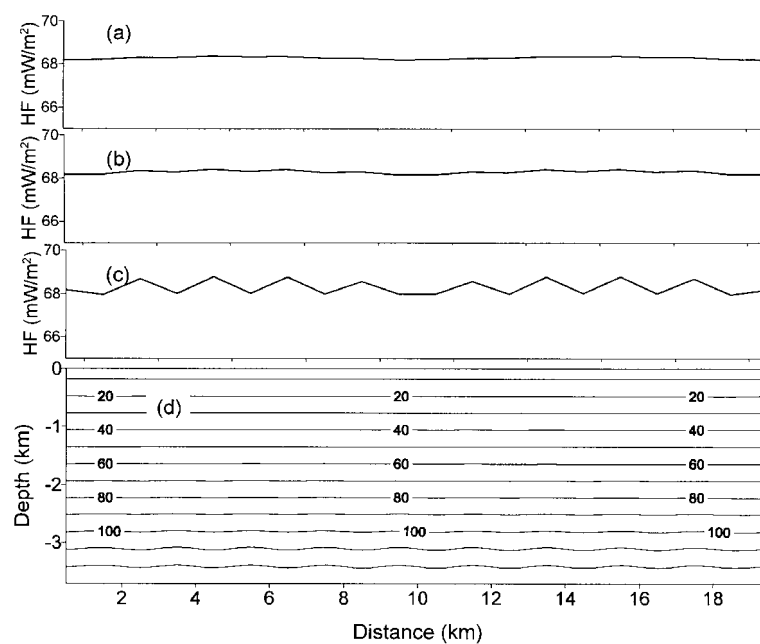

FIGURE 8:   Temperature field and heat flow distribution of model A; a) surface heat flow; b) the heat flow at 1 km depth; c) the heat flow at 2 km depth; d) temperature field

along the profile. As the depth increases, the effect of convection on the heat flow becomes more pronounced. At a depth of 1 km, the heat flow shows clear fluctuation although the amplitude is still very small. At a depth of 2 km, convective heat flow has become a relatively large part of the total heat flow, and cannot be ignored.

In model A, the surface heat flow is still controlled by conduction, and the convective disturbance is small enough to be ignored. Therefore, this model cannot explain the scatter of heat flow along the western transect.

5.2.2 Model B

Model B is the same as model A except that there are two vertical high-permeability zones, which are meant to simulate faults (Figure 9). They are 20 m wide, have a permeability of 5.0×10^{-14} m^2 and provide paths for water between the deep high-permeability layer and the surface. Fault 1 is close to the left boundary, whereas fault 2 is located centrally in the model. The initial condition is the stable temperature and pressure field obtained from model A. It is further assumed that, at time = 0, the two vertical faults are opened up (given high permeability).
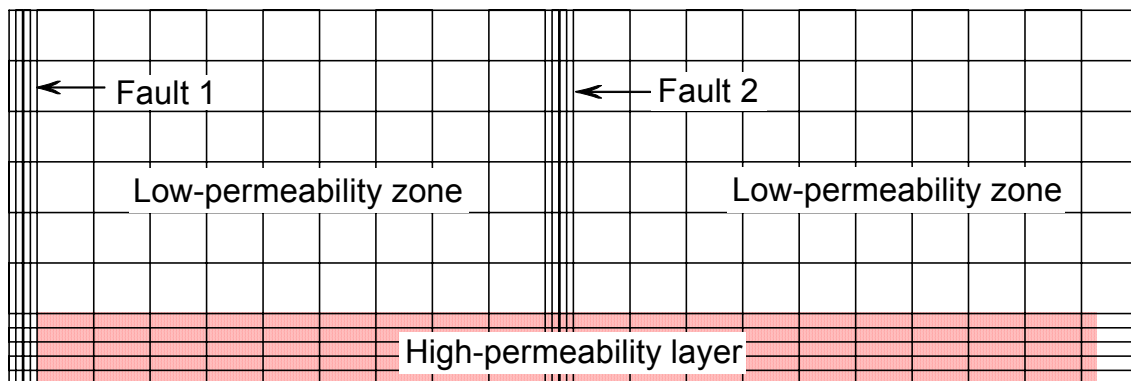

FIGURE 9:   Sketch of model B and grids used for modeling

FIGURE 10:   Variations in heat flow above faults in model B with time

Because of the open vertical zones, water will initially flow from the deep and locally over-pressurized high-permeability layer to the surface, increasing the surface heat flow above the fault zones in the process. The variations of surface heat flow with time above the faults are shown in Figure 10. After the fault opens, the surface heat flow above Fault 2 goes up immediately and reaches a peak value of 112 mW/m^2 within several years. Then it decreases gradually, with the rate of decrease slowing with time. During the period between years 500 to 1200, it is in a state of quasi-stability, in which the heat flow is 83mW/m^2, i.e. 15 mW/m^2 above the regional heat flow background. After that, the heat flow increases slowly again. The surface heat flow above Fault 1 shows a different behavior.
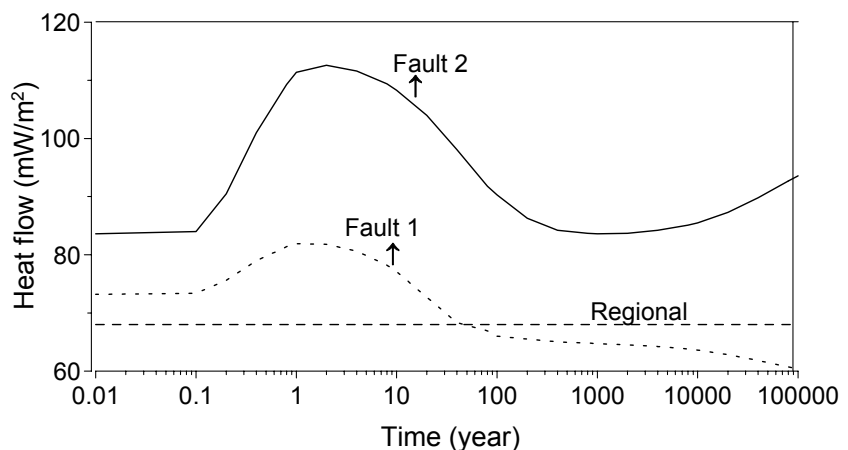
After the fault opens, the surface heat flow rises rapidly and reaches a peak value of 83 mW/m² within several years. It then decays gradually, and falls below the regional heat flow background 60 years later. During the period between years 500 and 1200, it also reaches a state of quasi-stability, with a value of 64 mW/m². After that, unlike the heat flow above the center fault, it decreases continuously. This is because large-scale hydrothermal circulation becomes exhibited. Cold water flows down fault 1, and hot water flows up to the surface through fault 2. Because the temperature differences between the near-surface layer (0-0.75 km, 4-30°C) and the cold sea water (4°C) are much less than those between the surface layer and the hot water (130°C) flowing up from the high-permeability layer, the cooling near the surface within fault 1 is much weaker than the heating within fault 2. This is the reason why the amplitude of the negative heat flow anomaly above fault 1 is much less than that of the positive heat flow anomaly above fault 2. In fact, the heat flow value is related closely with the permeability of the faults. Different faults may have different permeability, and different permeability can yield very different heat flow values.

The heat flow was next modeled for three different values of permeability in order to determine the effects of permeability. The results show that, for the center fault, the higher the permeability, the higher will be the heat flow (Figure 11). When the permeability is 5.0×10^{-14} m², the same as the permeability in the convection layer, the heat flow reaches an early maximum of 112 mW/m². If the permeability is increased to 7.0×10^{-14} m², the maximum increases to 130 mW/m². By contrast, if the permeability is lowered to 3.0×10^{-14} m², the highest heat flow falls to 96 mW/m². For fault 1, the heat flow responds to changes in permeability with time. In the first 100 years, the heat flow increases when permeability is increased, but later, the heat flow responds in the opposite direction. So, model B can
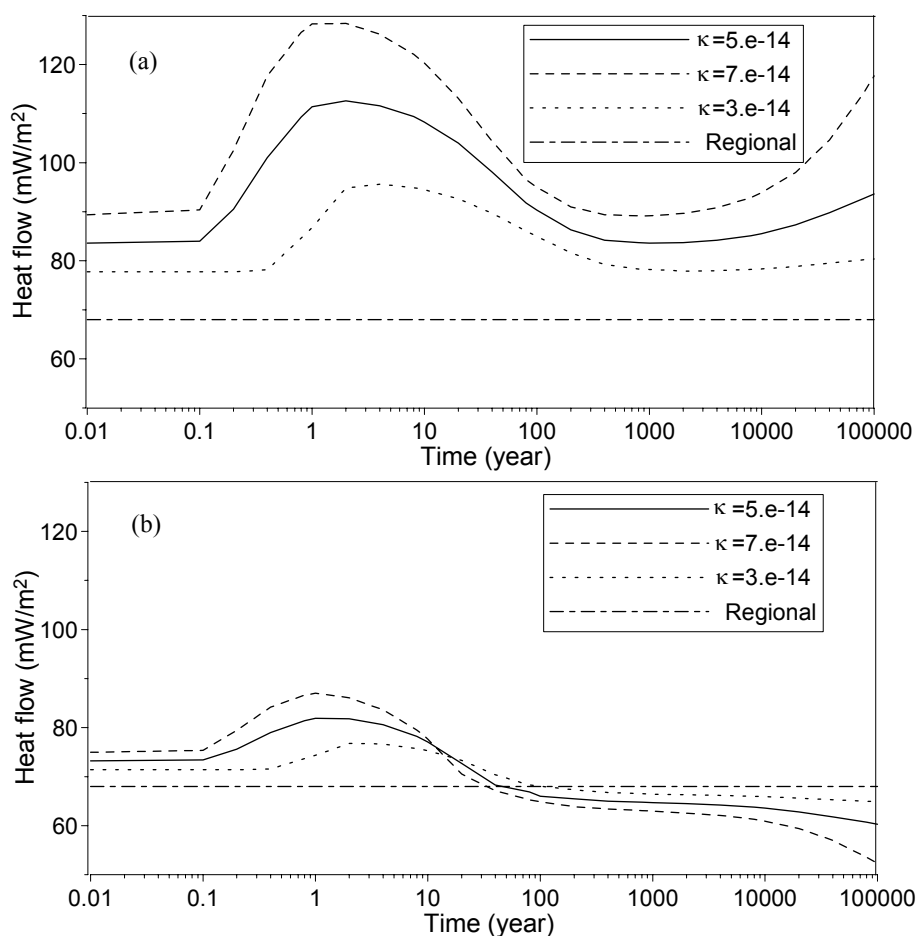

FIGURE 11: Variations in heat flow with time for different values
of permeability, a) heat flow above the central fault;
b) heat flow above the boundary fault

permeability is increased, but later, the heat flow responds in the opposite direction. So, model B can match a different range of observed heat flow values provided different permeabilities are assigned to the faults. From the modeling results, it is also evident that the hydrothermal circulation process can be divided into two stages. In the first stage, which is relatively short, hot water flows up through both of the faults, whereas in the second stage, which is relatively long, cold water flows down fault 1, and the hot water flows up from fault 2.
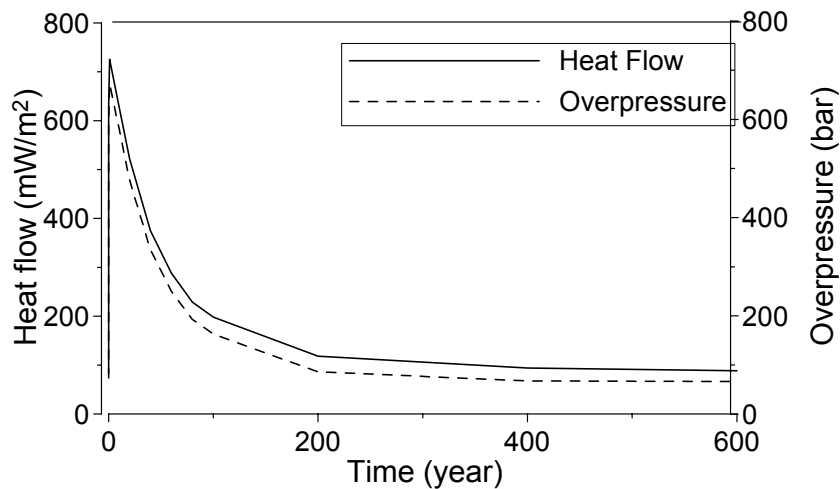
FIGURE 12: Variation of heat flow and pressure with time
assuming a 5-bar overpressure at depth prior to faulting

Deeply buried high-permeability, high-porosity layers are often overpressured and owe their existence to a lack of compaction, developed as a result of permeability barriers within the overburden. As the permeability barrier is broken by a fault, the overpressure is released. In order to simulate this process and its effects on the heat flow, the initial conditions were changed to a 5 bar overpressure in the high-permeability layer. As expected, the overpressure was released gradually after the fault opened, causing abnormally high heat flow. The heat flow then decayed with time synchronously with the pressure (Figure 12). Because of overpressure, the heat flow reached initially very high values of more than 700 mW/m^2. But as the pressure decayed, the heat flow also decreased and approached stable values on the time scale of hundreds of years.
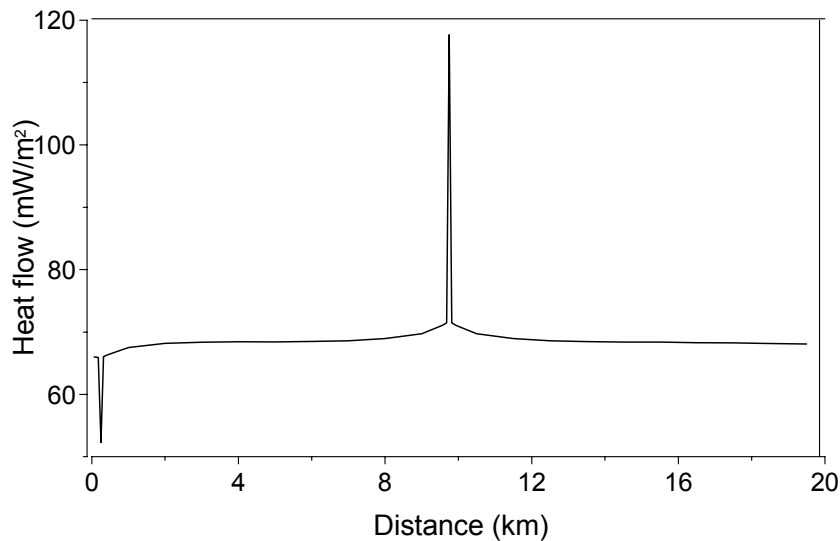

FIGURE 13: Heat flow to surface in model B

These results show that the opening up of a water-conducting fault between the high-permeability layer and the surface will influence the heat flow greatly. However, it is worth pointing out that the abnormally high heat flow only appears close to the narrow high-permeability fault zone (Figure 13). Beyond that, the surface heat flow is not visibly affected. So, abnormally high heat flow values are only encountered when the measurement station is close to a fault zone.

6. DISCUSSION

1. The western transect is very long and crosses several different tectonic provinces, such as the Pearl River Mouth basin and the Xisha Trough. The different provinces are characterized by different geological structures and stratigraphy. High permeability layers may or may not exist in the different provinces, and their thickness and depth may also vary. And more importantly, the permeability of existing fault zones may differ from one province to another. The construction of model B is based on borehole data from the Pearl River Mouth basin. It can be used to explain the scatter of heat flow data in this basin, and indicates a mechanism that might work in other areas, too.

2. In model B, the convection is controlled by the high-permeability layer at the base. It is unlikely that this high-permeability layer is present in the other areas, especially where the sedimentary cover is very thin. In this case, the question arises as to whether convection can occur in the basement? Miocene-Recent basalts are present in southern China (e.g., on Hainan Island and Leizhou Peninsula) and in Indiochina (Barr and MacD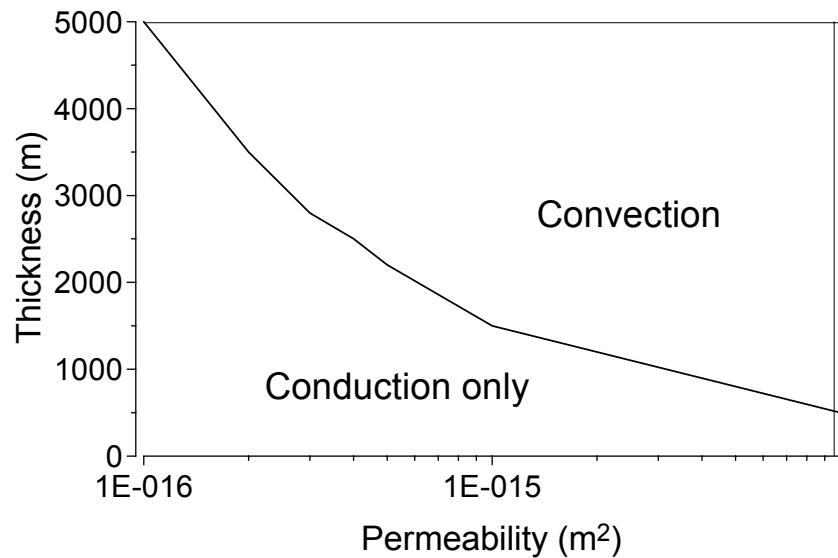onald, 1981). Basalts have also been identified in some wells in the Pearl River Mouth Basin (Li and Rao, 1994; Yu, 1994) and off western Taiwan (Chen, 1973; Yu, 1994). Oceanic basalts are estimated to have a permeability of about 10^{-16} m^2 (Turcotte and Schubert, 1982). If the thermal gradient is 40°C/km, a 5-km-thick layer of such permeability is needed to induce convection (Ra $\geq^3 40$). As the permeability increases, the layer thickness needed for free convection is greatly reduced (Figure 14). When the permeability is 1×10^{-16} m^2, a 2.2 km thick layer is enough to yield convection. If the permeability increases to 1×10^{-15} m^2 and 1×10^{-14} m^2, only 1.5 and 0.5 km thick layers are needed, respectively. So, convection is still possible in the upper crust where basalts of relatively high permeability are common.

FIGURE 14: Stability of conduction for different layer thickness and permeability

3. From model B we know that interlayer convection is not enough by itself to cause abnormally high or low heat flow. The presence of faults plays an important role. Few normal faults that cut through the entire crust have been observed along the western transect in the Xisha Trough and the Pearl River Mouth Basin (Hayes et al., 1995). These faults are associated with deep sedimentary basins, and there are indications that basement geology changes across the faults. But in model B, the faults need not be so large. Small faults or fissures are enough provided they have high permeability and cut through the conduction-dominated roof of the convection layer. Such small faults are pervasive in extensional regions.

4. Model B is a simple model. It does not include the complicated structure and large number of faults observed along the western transect. Its purpose is not to match every observed heat flow value, but to show the possibility of using hydrothermal circulation to explain the heat flow scatter. For the western transect, most of the heat flow values are between 60-80 mW/m², close to the regional heat flow background (Figure 15). Values below the background value fall into the 40-60 mW/m² range, whereas above the background value lie in 80-120 mW/m² range. In general, model B can explain the low heat flow
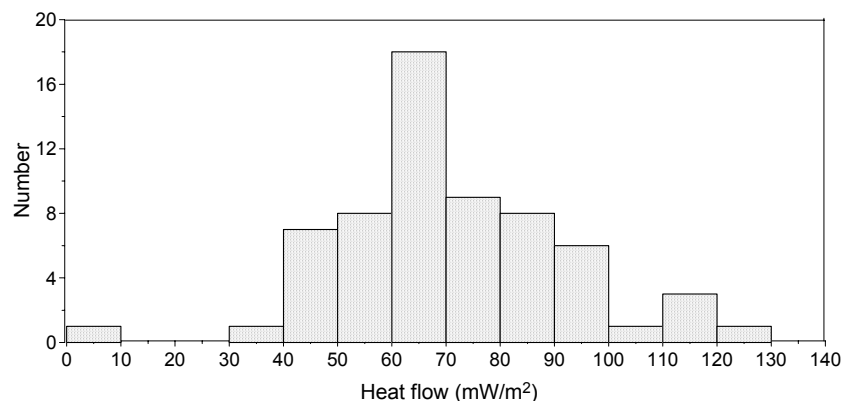

FIGURE 15: Heat flow histogram of the western transect

range as well as the high heat flow range, using the regional heat flow as background. Therefore, model B is able to explain the heat flow scatter. In order to fit the observed heat flow in detail, more data are needed on the permeability of sediments and basement, and the existence of small-scale faults and their permeability. This would be an appropriate subject for further investigation.

5. Besides hydrothermal convection, another likely explanation for the high heat flow values is the emplacement of igneous intrusions into the margin in recent time (5-1.5 Ma) (Nissen et al., 1995a). There is independent evidence that considerable igneous activity has occurred within the past 5 m.y. (e.g., Barr and MacDonald, 1981; Chen 1973). Nissen et al. (1995a) simulated the effects of magma intrusion on the heat flow. Four recent dike injections of different width at 2 Ma, 1.5 Ma and 5 Ma were put into their model. Assuming the position, width and age of the dikes, it was possible to account for the high heat flow values on the northern half of the western transect. However, unlike hydrothermal circulation, which can lower the apparent heat flow at some locations and elevate it at others, the intrusion of magma cannot explain the low heat flow values. So, a low average background heat flow is required if the heat flow scatter results only from the injection of igneous bodies into the crust (Nissen et. al., 1995a). But low background heat flow is inconsistent with the regional geothermal environment of the South China Sea basin, because the average heat flow along the western transect agrees well with the much better defined heat flow background values found in other parts of the South China Sea. Therefore, hydrothermal circulation is a more plausible explanation of the heat flow scatter.

7. CONCLUSION

A large number of heat flow measurements have been collected along the western transect. They provide valuable information for studying the geothermal conditions not only of the transect itself but also of the South China Sea basin. On one hand, the large number of data should enable more reliable inferences to be made. On the other hand, it also leads to difficulty in analysis, because the data are highly scattered. However, this challenge also provides an opportunity to better comprehend the complexities of the geothermal regime and mechanisms operating there.

1. Trend analysis using a 3rd order polynomial shows that the western transect is located in an area of high background heat flow. The heat flow increases from the northern margin into the deep-sea region, reaches its highest value in the Central Basin, and then decreases gradually. This feature is characteristic of rift basins. The average value is about 65-70 mW/m^2 at the northern margin, and 80 mW/m^2 in the central part of the transect.

2. In order to explain the scatter of the heat flow, a hydrothermal circulation mechanism was investigated with the help of TOUGH2 software. The results suggest that hydrothermal convection within a highly permeable layer, linked to the surface through open faults, can elevate the heat flow in some areas and lower it in others. This is a possible explanation of the observed heat flow scatter.

3. Since detailed data on permeability and the location and structure of faults is lacking, the model is unavoidably somewhat speculative and simple, but it indicates that hydrothermal circulation may play an important role in the geothermal regime of the South China Sea Basin.

ACKNOWLEDGMENTS

REFERENCES

Barr, S.M., and MacDonald, A.S., 1981: Geochemistry and geochronology of late Cenozoic basalts of Southeast Asia. *Geol. Soc. Am. Bull., 92*, 1069-1142.

Chen, J.C., 1973: Geochemistry of basalts from Penghu Islands. *Proc. Geol. Soc. China, 16*, 23-26.

Crane, K., 1979: Hydrothermal stress drops and convective patterns at three mid-ocean spreading centers. *Tectonophysics, 55,* 215-238.

Fehn, U. and Cathles, L.M., 1979: Hydrothermal convection at slow-spreading mid-ocean ridges. *Tectonophysics, 55,* 239-260.

Hayes, D.E., Nissen S.S., Buhl, P., Diebold, J., Yao B., Zeng W., and Chen Y., 1995: Throughgoing crustal faults along the northern margin of the South China Sea and their role in crustal extension. *J. Geophys. Res., 100-B11*, 22435-22446.

He Lijuan, Xiong Liangping and Wang Jiyang, 1998: Geothermal Characteristics of South China Sea. *China Offshore Oil and Gas (Geology) 12 (in Chinese)*, 87-90.

He Lijuan, Xiong Liangping, Wang Jiyang and Wang Kelin, 1995: Computation of stretch factors in modeling multiple stretch basins. *Chinese Science Bulletin 40 (24) (in Chinese)*, 2261-2263.

Li Pinglu and Rao Chuntao, 1994: Tectonic characteristics and evolution history of the Pearl River Mouth Basin. *Tectonophysics, 235*, 13-25.

Nissen, S. S., Hayes D. E., Yao Bochu, Zeng Weijun, Chen Yongqin and Nu Xianpin, 1995a: Gravity, heat flow, and seismic constraints on the processes of crustal extension: Northern margin of the South China Sea. *J. Geophys. Res., 100-B11,* 22447-22483.

Nissen S.S., Hayes D.E., Buhl P., Diebold J., Yao Bochu, Zeng Weijun and Chen Yongqin, 1995b: Deep penetration seismic soundings across the northern margin of the South China Sea. *J. Geophys. Res., 100-B11,* 22407-22433.

Pruess, K., 1991: *TOUGH2 – A general purpose numerical simulator for multiphase fluid and heat flow*. Lawrence Berkeley Laboratory, Berkeley. CA, report LBL-29400,159 pp.

Rybach, L., and Muffler L.J.P., 1981: *Geothermal systems: Principles and case histories*. John Wiley & Sons Ltd., 359 pp.

Turcotte D.L., and Schubert G., 1982*: Geodynamics, applications of continuum physics to geological problems*, John Wiley & Sons, NY, 433 pp.

Wang Jiyang, Xiong Liangping and Pang Zhonghe, 1993: *Low-, medium-temperature geothermal systems of convective type*. Science press, Beijing (in Chinese), 240 pp.

Wessel P., and Smith, H., 1995: *The generic mapping yools (GMT), version 3. Technical reference and cookbook*.   School Ocean and Earth Science Technology/National Ocean and Atmospheric Administration, 77 pp.

Yao Bochu, Zeng Weijun, Hayes D. D., and Nissen S. S., 1994: *The geological memoir of South China Sea surveyed jointly by China & USA*. China University of Geosciences Press, Beijing (in Chinese), 240 pp.

Yu, H.S., 1994: Structure, stratigraphy and basin subsidence of Tertiary basins along the Chinese southern continental margin. *Tectonophysics, 235*, 63-76.